Using Computational Fluid Dynamics Analysis to Characterize Local Hemodynamic Features of Middle Cerebral Artery Aneurysm Rupture Points

Keiji Fukazawa[1], Fujimaro Ishida[1], Yasuyuki Umeda[2], Yoichi Miura[2], Shinichi Shimosaka[1], Satoshi Matsushima[2], Waro Taki[2], Hidenori Suzuki[2]

Key words
- Computational fluid dynamics
- Local hemodynamics
- Rupture point
- Ruptured cerebral aneurysm
- Wall shear stress

Abbreviations and Acronyms
3D-CTA: Three-dimensional computed tomographic angiography
CFD: Computational fluid dynamics
CT: Computed tomography
MCA: Middle cerebral artery
NWSS: Normalized wall shear stress
WSS: Wall shear stress

From the [1]Department of Neurosurgery, NHO Mie Chuo Medical Center, Mie; and [2]Department of Neurosurgery, Mie University Graduate School of Medicine, Tsu, Mie, Japan

To whom correspondence should be addressed: Keiji Fukazawa, M.D. [E-mail: fukaz1977@yahoo.co.jp]

Citation: World Neurosurg. (2015) 83, 1:80-86.
http://dx.doi.org/10.1016/j.wneu.2013.02.012

Journal homepage: www.WORLDNEUROSURGERY.org

Available online: www.sciencedirect.com

OBJECTIVE: **Although rupture of cerebral aneurysms typically occurs at the fragile wall at the apex or pole, some aneurysms rupture through the body or the neck. The purpose of this study was to clarify the association between aneurysm rupture points and hemodynamic features through the use of computational fluid dynamics (CFD) analysis.**

METHODS: **Twelve ruptured middle cerebral artery bifurcation aneurysms were analyzed by 3-dimensional computed tomographic angiography and CFD. Rupture points were evaluated on intraoperative videos by 3 independent neurosurgeons. Wall shear stress (WSS) was calculated at the rupture point, aneurysm dome, and parent artery. Intra-aneurysmal flow patterns were evaluated with cross-sectional velocity vector planes that included the rupture points.**

RESULTS: **The mean WSS at the rupture point (0.29 Pa) was significantly lower than that at the dome (2.27 Pa) and the parent artery (8.19 Pa) ($P < .01$). All rupture points were located within the area of WSS ≤ 11.2% of the WSS at the parent artery. WSS at the rupture point was correlated with the minimum WSS at the dome ($r = 0.64$, $P < .05$), but not with aneurysm size ($r = 0.26$) or the aspect ratio ($r = 0.16$). Flow patterns revealed that all rupture points were located in lower-velocity area, which was associated with complex flow patterns and/or deviating necks.**

CONCLUSIONS: **This study highlights the relationship between the local hemodynamic features and the rupture points observed during the microsurgical clipping. CFD may determine a rupture point of aneurysms using the feature of markedly low WSS.**

INTRODUCTION

Noninvasive cerebrovascular imaging techniques, such as magnetic resonance angiography and 3-dimensional computed tomographic angiography (3D-CTA), have detected unruptured cerebral aneurysms with high sensitivity (26). Although some previous studies focus on aneurysm diameter and location to predict aneurysm rupture, these simple parameters have limitations, including its poor interaction with hemodynamic variables (24, 27). Indeed, recent studies using computational fluid dynamic (CFD) techniques have demonstrated that hemodynamic features are possible key parameters for aneurysm growth and rupture (1-4, 8, 11, 12, 17, 18, 21-23, 28). If hemodynamic factors contribute to aneurysm rupture as reported previously, it is hypothesized that there would be unique hemodynamic features around the rupture point. To our knowledge, however, local hemodynamic features of rupture sites have not been previously or fully examined with CFD analysis. Thus, the goal of the present study was to use CFD analysis based on patient-specific models obtained from preoperative 3D-CTA to characterize the relationship between hemodynamic features and the aneurysmal rupture point observed during microsurgical clipping.

METHODS

Patient Population

From April 2007 to March 2010, 60 ruptured middle cerebral artery (MCA) aneurysms were diagnosed by 3D-CTA, and clipping surgeries were performed in 58 cases. Among them, 12 aneurysms ranging in size from 3.3 to 13.6 mm (mean size, 7.8 mm) were analyzed in this study, because the 12 aneurysms satisfied the following criteria for inclusion: 1) detection of the apparent rupture point during clipping surgery, 2) availability of preoperative 3D-CTA with adequate image quality for generation of a geometry model, and 3) the dome volume that could be distinguished from the middle cerebral parent artery volume through the use of an intersecting plane (Figure 1A) (21). Another 46 aneurysms were excluded due to failed detection of an apparent rupture point during surgery (n = 34) and/or poor imaging quality (n = 12).

Image Acquisition

Preoperative 3D-CTA were performed with a 64-detector multislice computed

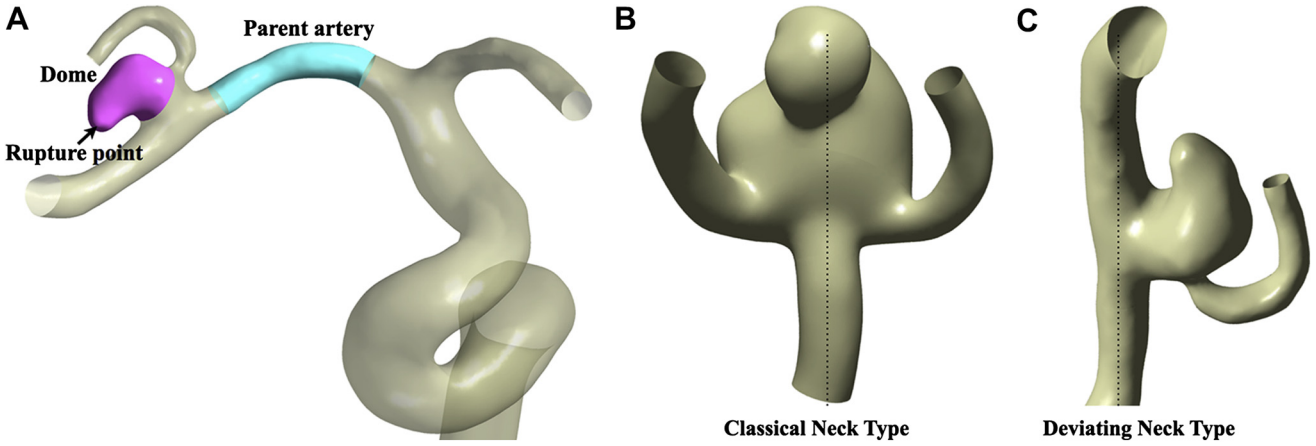

Figure 1. (**A**) Definition of neck geometry; (**B**) classic neck type, showing that the central axis of the parent artery crosses the line of the neck; (**C**) deviating neck type, showing that the central axis of the parent artery does not cross the line of the neck.

tomography (CT) scanner (Aquillion 64; Toshiba, Inc., Tokyo, Japan). Study parameters included radiation parameters 300 mA and 120 kV, matrix size 512 × 512, field of view 32 cm, slice thickness 0.5 mm, helical pitch 1.0, and isotropic voxel size 0.5 mm. A 100-mL dose of nonionic contrast medium (Omnipaque 370; Daiichi-Sankyo Pharmaceutical Co., Tokyo, Japan) was delivered into the right antecubital vein by means of a power injector at the rate of 5 mL/s. The initiation of scanning was set with a real-time bolus-tracking system (Sure Start; Toshiba, Inc., Tokyo, Japan). For each aneurysm, the neck width and the maximum height of the dome were measured from the 3D-CTA, and the aspect ratio (25) was determined.

Model Construction

The surface of the arterial lumen was constructed first by using commercially available software packages (Magics 13.0 and Mimics 14.0; Materialise Japan, Yokohama, Japan). Arterial lumen was segmented based on intra-arterial CT values to convert the Digital Imaging and Communication in Medicine dataset into stereolithography. In addition, smoothing of Laplace transform was performed. The surface geometry was divided into dome and parent artery with an intersecting plane (Figure 1A). The computational meshes were generated for these models using commercial software (ANSYS ICEM CFD12.1; ANSYS Inc., Canonsburg, PA, USA). Element sizes ranged between 0.1 and 0.7 mm, with smaller elements in high curvature regions. Three prismatic boundary layers with a total thickness of 0.15 mm covered the vessel wall to locally ensure an accurate definition of the velocity gradient. A straight inlet extension was added to the C5 segment of the internal carotid artery to obtain fully developed laminar flow. On average, meshes consisted of 230,000 nodes and 580,000 tetrahedral and prismatic elements.

Numerical Modeling

For the fluid domain, 3D incompressible laminar flow fields were obtained by solving the continuity and Navier-Stokes equations. Numerical modeling was performed using a commercially available CFD package (ANSYS CFX12.1; ANSYS Inc., Canonsburg, PA, USA). Vessel walls were assumed to be rigid, and no slip boundary conditions were applied at the walls. Blood was assumed to be an incompressible Newtonian fluid with a blood density of 1056 kg/m^3 and a blood dynamics viscosity of 0.0035 N/m^2/s. Because patient-specific flow information was not available, pulsatile boundary conditions were based on the superposition blood-flow waveforms of the common carotid artery as characterized by Doppler ultrasound in normal human subjects for transient analysis (9). Traction-free boundary conditions were applied at outlets of the MCA and the anterior cerebral artery (20). The time steps were 0.005 seconds. To reduce initial transients, we computed 3 cardiac cycles, and data of the third cardiac cycle were analyzed. Hemodynamic results of the flow field were examined at end-diastole.

Definition of Geometry

Three independent neurosurgeons evaluated the operation videos blindly to the CFD findings. The rupture point was detected as tight adhesion to hematoma or white thrombus, thin wall, and disruption of the aneurysmal wall (10). After the detection of a rupture point on the operation video, each neurosurgeon determined each location of the rupture point on the patient-specific geometry model. Apparent differences in assessment were resolved by consensus, and if differences were not resolved by consensus, the cases were excluded from the study. The dome was cut around the neck with the intersecting plane, and the M1 segment was defined as the parent artery (Figure 1A). In addition, neck types were classified into 2 types based on neck location. Thus, when the aneurysmal neck was located on the extension of the midline axis of the parent artery, it was defined as a classic neck type (Figure 1B), and when it was not, it was defined as a deviating neck type (Figure 1C). In deviating neck types, relationships among a rupture point, the side of a deviating neck, and the flow dynamics were investigated.

Flow Structure Analysis

Flow structures were investigated with a cross-sectional vector velocity plane including the rupture point and with 3D streamlines of intra-aneurysmal flow.